International Journal of Heat and Mass Transfer 52 (2009) 2581–2588

Contents lists available at ScienceDirect

International Journal of Heat and Mass Transfer

journal homepage: www.elsevier.com/locate/ijhmt

Frost behavior on a fin considering the heat conduction of heat exchanger fins

Jung-Soo Kim, Kwan-Soo Lee *, Se-Jin Yook

School of Mech. Eng., Hanyang University, Sungdong-gu, Seoul 133-791, Republic of Korea

ARTICLE INFO

Article history:
Received 23 August 2008
Received in revised form 17 December 2008
Available online 27 February 2009

Keywords:
Fin heat conduction
Frost behavior
Heat exchanger fins

ABSTRACT

A mathematical model is proposed for predicting frost behavior on a heat exchanger fin under frosting conditions, taking into account fin heat conduction. The change in the three-dimensional airside airflow caused by frost growth is reflected in this model. The numerical estimates of frost thickness are consistent with experimental data, with an error of less than 10%. Due to fin heat conduction, frost thickness decreases exponentially toward the fin tip, while considerable frost growth occurs near the fin base. When a constant fin surface temperature is assumed, the predicted frost thickness was larger by more than 200% at maximum, and the heat flux by more than 10% on average, compared to results obtained with fin heat conduction taken into account. Therefore, fin heat conduction could be an essential factor in accurately predicting frost behavior. To improve prediction accuracy under the assumption of constant fin surface temperature, the equivalent temperature (for predicting frost behavior) is defined to be the temperature at which the heat transfer rate neglecting fin heat conduction is the same as the heat transfer rate with fin heat conduction taken into consideration. Finally, a correlation for predicting the equivalent temperature is suggested.

1. Introduction

When water vapor contacts the fins of a heat exchanger operating at low temperatures, a porous frost layer accumulates on the cold surface. The frost layer contributes to the increase in both thermal and flow resistances as operating time elapses, thus degrading the thermal performance of the heat exchanger. Therefore, both the behavior of the frost formed on the fin and the characteristics of the heat and mass transfer must be accurately predicted in designing effective heat exchangers.

The study of frost formation on heat exchangers can be accomplished by two different approaches: a macroscopic point of view and a microscopic perspective. The first approach, which has already appeared in numerous studies [1–5], focuses on the performance evaluation of the entire system, making it difficult to predict local frost behavior. The second approach provides a detailed consideration of frost formation phenomena on cold surfaces, so that the results can be applied to heat exchangers. Most studies [6–12] have proposed mathematical models for predicting the behavior of frost forming on a cold surface by assuming a constant fin surface temperature. However, the results of these studies differ from cases that consider a nonuniform temperature distribution along the fin. Recently, some studies [13–16] have analyzed frost formation phenomena on a fin by considering fin heat conduction. Chen et al. [13] analyzed frost behavior on heat exchanger fins by using a local volume-averaging technique proposed by Tao et al. [12], and compared their results with the experimental data of Chen et al. [14]. Tso et al. [15] proposed an improved model for predicting the performance of finned tube heat exchangers with frost thickness variations along the fins by converting a rectangular fin into an equivalent angular fin. However, these studies [13,15] did not consider the change in the airside airflow caused by frost growth. Xia and Jacobi [16] proposed an exact solution to steady heat conduction in a two-dimensional (2D) slab on a one-dimensional fin, but this study considered heat conduction within the composite medium, and had no bearing on the prediction of frost behavior by frosting analysis.

This paper proposes a mathematical model for predicting frosting behavior on a heat exchanger fin under frosting conditions, taking fin heat conduction into account. The change in three-dimensional (3D) airside airflow caused by frost growth is reflected in this model. A frosting experiment is carried out to validate the model. We predict frost formation phenomena on a fin with a nonuniform temperature distribution, and compare frost behavior with and without fin heat conduction.

2. Theoretical study

2.1. Physical model

Fig. 1 shows the configuration of a plate-fin heat exchanger, with the fins placed parallel to the airflow direction. Taking the

* Corresponding author. Tel.: +82 2 2220 0426; fax: +82 2 2295 9021.
E-mail address: ksleehy@hanyang.ac.kr (K.-S. Lee).

0017-9310/$ - see front matter Crown Copyright © 2009 Published by Elsevier Ltd. All rights reserved.
doi:10.1016/j.ijheatmasstransfer.2008.12.023

Nomenclature

c_p	specific heat (J/kg K)
D_w	mass diffusivity (m^2/s)
Fo	Fourier number, $\alpha_a t_{op}/L_{fin}^2$
H_{fin}	fin height (m)
h_h	heat transfer coefficient (W/m^2 K)
h_m	mass transfer coefficient (kg/m^2 s)
h_{sv}	latent heat of sublimation (J/kg)
k	thermal conductivity (W/mK)
k_{eff}	effective thermal conductivity (W/mK)
L_{fin}	fin length (m)
m_w	mass concentration of vapor
$\dot{m}_y$	mass flux for frost thickness (kg/m^2 s)
$\dot{m}_\rho$	mass flux for frost density (kg/m^2 s)
P	pressure (Pa)
q_{tot}	total heat flux (W/m^2)
Re_L	Reynolds number, $u_a L_{fin}/\nu$
T	temperature (K)
T_{eq}	equivalent temperature (K)
t_{fin}	fin thickness (m)
t_{op}	operating time (min)
u	air velocity (m/s)
w	absolute humidity (kg/kg_a)
y_f	frost thickness (m)

Greek symbols

α_f	absorption coefficient (m^2/s)
Δ	increment
ν	dynamic viscosity (m^2/s)
ρ	density (kg/m^3)

Superscript

*	dimensionless

Subscripts

a	air
b	fin base
f	frost
fs	frost surface
in	inlet
out	outlet
sat	saturation
t	time

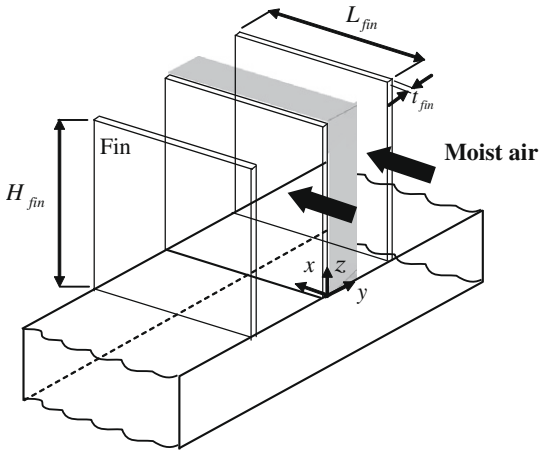

Fig. 1. Configuration of a heat exchanger.

array of heat exchanger fins and the flow characteristics into consideration, we simulated frost behavior on only one fin instead of all the fins, as depicted by the shaded region in Fig. 1. For the simulation, the following assumptions were made:

(1) The airflow was 3D, incompressible, and laminar.
(2) The effect of gravity was negligible.
(3) The frosting process proceeded in a quasi-steady state.
(4) The thermal conductivity of the fin was constant.
(5) The temperature distribution of the fin was 2D, i.e. $T_{fin}(x,z)$.

2.2. Mathematical model

The frosting model consisted of an airside, frost layer, and fin model, and these were coupled together. We added fin heat conduction to the existing model (i.e. an airside with a 2D airflow and a frost layer) and extended the airside model to a 3D airflow field to make accurate predictions about the frost formed on the fin.

2.2.1. Airside

The laminar flow equation was employed to determine the change in 3D airside airflow caused by frost growth. The governing equation is expressed in tensor form as

$$\frac{\partial}{\partial x_i}(\rho u_i \phi) = \frac{\partial}{\partial x_i}\left(\sigma_\phi \frac{\partial \phi}{\partial x_i}\right) + S_\phi \tag{1}$$

where ϕ is the dependent variable, and σ_ϕ and S_ϕ are the diffusion coefficient and source term corresponding to the dependent variable, respectively, as listed in Table 1.

Eq. (1) was subject to the boundary conditions shown in Fig. 2, and the conditions were grouped by inlet/outlet, symmetry, and wall/interface boundaries.

2.2.1.1. Inlet and outlet boundaries. The working conditions of the airflow were set as the inlet conditions. For the outlet, a zero-gradient condition was imposed. These conditions are as follows:

$$\text{Inlet}: \quad u = u_{in}, \quad v = 0, \quad w = 0, \quad T = T_{in}, \quad m_w = m_{w,in} \tag{2a}$$

$$\text{Outlet}: \quad \frac{\partial u}{\partial x} = 0, \quad \frac{\partial v}{\partial x} = 0, \quad \frac{\partial w}{\partial x} = 0, \quad \frac{\partial T}{\partial x} = 0, \quad \frac{\partial m_w}{\partial x} = 0 \tag{2b}$$

2.2.1.2. Symmetry boundaries. Taking the array of heat exchanger fins and flow characteristics into consideration, symmetry conditions were imposed in the following planes:

$$\text{Front plane}, y = 0: \quad \frac{\partial u}{\partial y} = 0, \quad \frac{\partial v}{\partial y} = 0, \quad \frac{\partial w}{\partial y} = 0, \quad \frac{\partial T}{\partial y} = 0, \quad \frac{\partial m_w}{\partial y} = 0 \tag{2c}$$

$$\text{Rear plane}, y = W: \quad \frac{\partial u}{\partial y} = 0, \quad \frac{\partial v}{\partial y} = 0, \quad \frac{\partial w}{\partial y} = 0, \quad \frac{\partial T}{\partial y} = 0, \quad \frac{\partial m_w}{\partial y} = 0 \tag{2d}$$

2.2.1.3. Wall and interface boundaries. A no-slip boundary condition was imposed for all surfaces including an air–frost interface. The wall was assumed to be adiabatic. At $y = 0$ and $z = 0$, the fin base

Table 1
ϕ, σ_ϕ and S_ϕ for Eq. (1).

Equation	ϕ	σ_ϕ	S_ϕ
Continuity	1	–	0
u-Momentum	u	μ	$-\frac{\partial P}{\partial x}$
v-Momentum	v	μ	$-\frac{\partial P}{\partial y}$
w-Momentum	w	μ	$-\frac{\partial P}{\partial z}$
Energy	T	k_a/c_p	0
Mass concentration	m_w	ρD_w	0

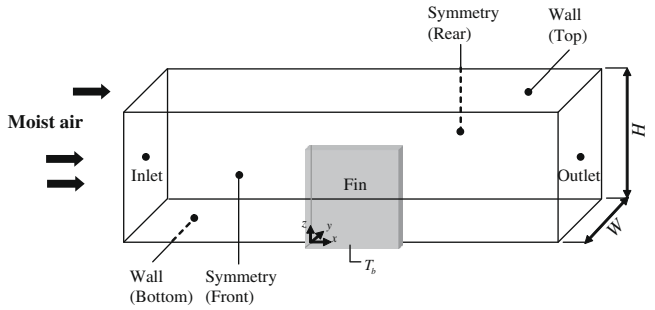

Fig. 2. Boundary conditions.

temperature (T_b), along with the direction of airflow, was held constant. The water vapor on the cold plate and interface was regarded to be saturated.

$$\text{Bottom plane, } z=0: \; u=0, \quad v=0, \quad w=0, \quad \partial T/\partial z=0, \quad \partial m_w/\partial z=0 \tag{2e}$$

$$\text{Top plane, } z=H: \; u=0, \quad v=0, \quad w=0, \quad \partial T/\partial z=0, \quad \partial m_w/\partial z=0 \tag{2f}$$

$$\text{Cold plate (fin)}: \; u=0, \quad v=0, \quad w=0, \quad T_{\text{fin}}(x,y=0,z=0)=T_b, \quad m_w=m_{w,\text{sat}}(T_{\text{fin}}) \tag{2g}$$

$$\text{Air-frost interface, } y=y_f: \; u=0, \quad v=0, \quad w=0, \quad T=T_{fs}, \quad m_w=m_{w,\text{sat}}(T_{fs}) \tag{2h}$$

2.2.2. Frost layer

The governing equations for predicting frost growth are those of heat and mass transfer. The water vapor diffusion equation and heat transfer equation in the frost layer are expressed as follows [8]:

$$D_w\frac{\partial^2\rho_w}{\partial y^2}=\alpha_f\rho_w \tag{3}$$

$$k_{\text{eff}}\frac{\partial^2 T_f}{\partial y^2}=-\alpha_f\rho_w h_{sv} \tag{4}$$

where D_w is the diffusion coefficient of water vapor and α_f is an absorption coefficient. The effective thermal conductivity (k_{eff}) of the frost layer is a function of the frost density only, as described by Lee et al. [8].

The total heat transfer was the sum of the sensible and latent heat between the moist air and the frost surface.

$$q_{\text{tot}}=q_{\text{sen}}+q_{\text{lat}}=h_h(T_a-T_{fs})+h_m(w_a-w_{fs})h_{sv} \tag{5}$$

The water vapor absorbed into the frost surface from the moist air was diffused within the frost layer, resulting in an increase in both frost thickness and frost density.

$$\dot m_f=\rho_a D_w\left.\frac{\partial m_w}{\partial y}\right|_{y_f}=\dot m_y+\dot m_\rho \tag{6}$$

The frost thickness and the frost density at a given time step were calculated from

$$y_f\big|_{t+\Delta t}=y_f\big|_t+\left.\frac{\dot m_y}{\rho_f}\right|_t\Delta t \tag{7a}$$

$$\rho_f\big|_{t+\Delta t}=\rho_f\big|_t+\left.\frac{\dot m_\rho}{y_f}\right|_t\Delta t \tag{7b}$$

2.2.3. Fin model

Fig. 3 shows a schematic diagram depicting the heat conduction model on a 2D fin surface. The fin heat conduction model was coupled with the frost layer model as follows:

$$k_{\text{fin}}\left(\frac{\partial^2 T_{\text{fin}}}{\partial x^2}+\frac{\partial^2 T_{\text{fin}}}{\partial z^2}\right)+S=0, \quad S=\frac{2}{t_{\text{fin}}}k_{\text{eff}}\left.\frac{\partial T_f}{\partial y}\right|_{y=0} \tag{8}$$

where S is the heat transfer rate from the frost layer into the fin, and the factor of 2 accounts for the frost growth on both sides of the fin. As the boundary conditions for this fin heat conduction model, a constant temperature was specified at the fin base, and the other three edges were assumed adiabatic because of the thinness of the fin.

$$T_{\text{fin}}(x,y=0,z=0)=T_b \tag{9a}$$

$$\frac{\partial T_{\text{fin}}(x,y=0,z=H_{\text{fin}})}{\partial z}=0 \tag{9b}$$

$$\frac{\partial T_{\text{fin}}(x=0,y=0,z)}{\partial x}=0 \tag{9c}$$

$$\frac{\partial T_{\text{fin}}(x=L_{\text{fin}},y=0,z)}{\partial x}=0 \tag{9d}$$

2.3. Numerical analysis

We conducted a numerical analysis using the SIMPLER algorithm, and employed nonuniform and staggered grids to ensure the accuracy of the solution. We also used variable-grid methods to resolve the moving boundary problem caused by frost growth [17]. These methods used equal time steps and maintained a fixed number of space intervals during the operating time to allow the size of the space interval to change in accordance with the moving air–frost interface. A grid independence test was performed by changing the number of grid points, until the changes in frost thickness and heat transfer rate were less than 1%.

To begin with, the primary values, such as operating conditions and initial conditions, were assumed. The initial temperature distribution on the fin was computed on the basis of fin heat conduction, and the equations governing both the airside and the frost layer were solved simultaneously. The heat and mass transfer rates

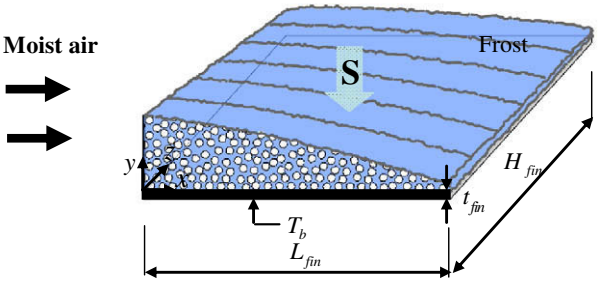

Fig. 3. Schematic diagram of fin heat conduction model.

were computed iteratively until an energy balance was attained at the air–frost interface [9]. With the frost surface temperature stabilized, we calculated frost properties such as frost thickness and frost density at each grid point. These frost properties were inserted into the fin heat conduction model to obtain a new temperature distribution, which was then used as a new boundary condition for the next time step to solve the governing equations for the airside and frost layer. This procedure was repeated during the given operation time.

3. Experiment

A frosting experiment was performed to validate the frosting model described above. The test conditions were $7 \leqslant T_a \leqslant 10\ ^\circ C$, $1.0 \leqslant u_a \leqslant 1.5$ m/s, $0.00371 \leqslant w_a \leqslant 0.00569$ kg/kg$_a$ and $-20 \leqslant T_b \leqslant -25\ ^\circ C$.

The experimental apparatus was composed of four sections [9]: a climate chamber for controlling the humidity and temperature of the inlet air, a cooling section for controlling the temperature and flow rate of the refrigerant, a test section for measuring the frost layer on the fins of a heat exchanger, and a circulation section connecting each section to recirculate the moist air.

Fig. 4 shows the schematic diagram of test section of which size was 300 × 150 × 150 mm. The heat exchanger (HEX) was placed at the center of the test section. Holes were drilled on two sides of the test section for the measurement of frost thickness. The holes were made as small as possible in order to minimize the measurement error caused by the entry of ambient air through the holes during measurements.

The heat exchanger fins were initially plastic-wrapped to prevent frost formation on the fin while stabilizing the experimental conditions. When the operating conditions reached a steady state, the frosting experiment was initiated by detaching the wrap from the fins. Each experiment was repeated more than five times. Fin surface temperature and frost thickness were measured at the distances of z = 17.5, 35, and 52.5 mm away from the fin base when x = 30 mm, and at the positions of x = 15, 30, and 45 mm away from leading edge of the fin when z = 35 mm. The fin surface temperature was measured by type T thermocouples, and the frost thickness was measured using a digital micrometer [18].

The uncertainties [19] of the base and surface temperatures of the fin were found to be within ±0.34 and ±0.31 °C, respectively. The uncertainty of the frost thickness was ±0.04 mm.

4. Results and discussion

The frosting model proposed in this study was validated by comparing numerical and experimental data. Fig. 5 shows the comparison of the fin surface temperature on 2D fin, in the airflow direction and the direction perpendicular to airflow. The temperature distribution of 2D fin was consistent with the experimental data. Fig. 6 shows the comparison of the transient frost thickness on 2D at different humidity ratios. The numerical predictions of the frost thickness were in close agreement with the experimental data, with the error less than 10%.

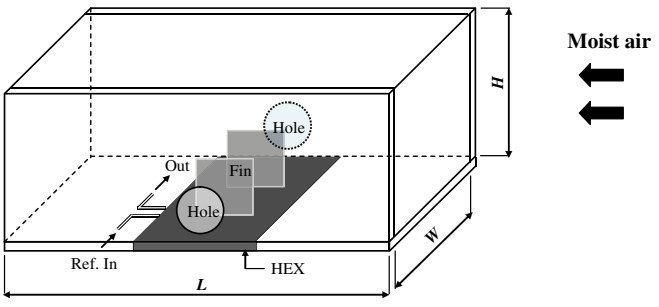

Fig. 4. Schematic diagram of test section.

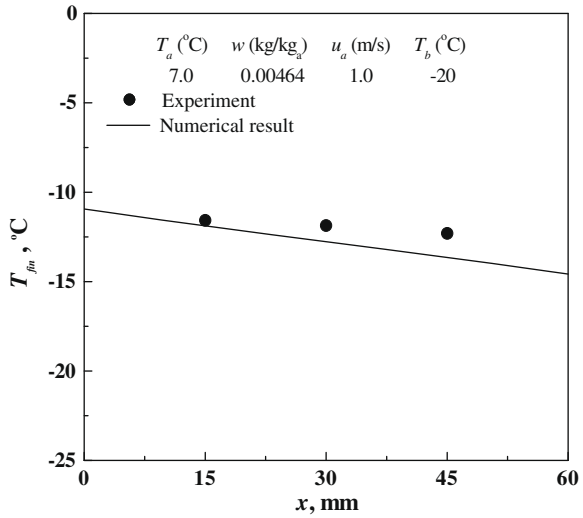

(a) The airflow direction at z = 35 mm

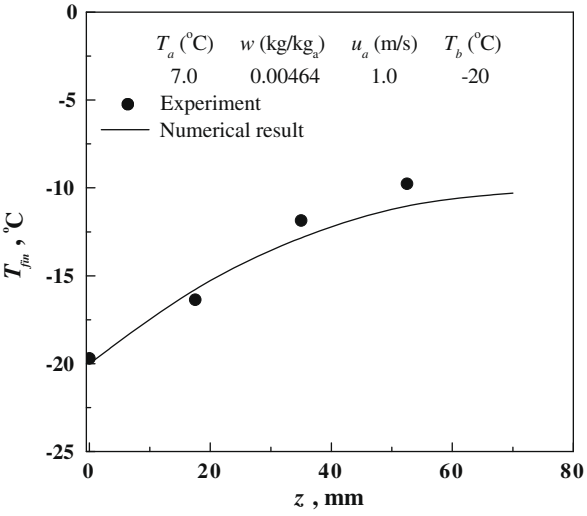

(b) The direction perpendicular to airflow at x = 30 mm

Fig. 5. Comparison of fin surface temperature between numerical results and experimental data at t = 90 min.

4.1. Frost behavior

The fin used in this study was 60-mm-long, 70-mm-high, and 1-mm-thick. Thermal conductivity of the fin was 220 W/mK. The temperature distribution of a heat exchanger fin is closely related to both the frost behavior and the characteristics of heat and mass transfer. Fig. 7 shows the temperature contours on a 2D fin surface at given conditions. The temperature distribution was nonuniform as a result of the fin heat conduction. The temperature at the fin base (z = 0 mm) was constant while the fin surface temperature increased toward the fin tip (z = 70 mm). However, the temperature gradient in the x-direction (i.e. the airflow direction) was small throughout the entire fin, since it was mostly affected by changes in the properties of the moist air. In particular, little variation was observed in the temperature gradient near the fin base, where temperature was constant.

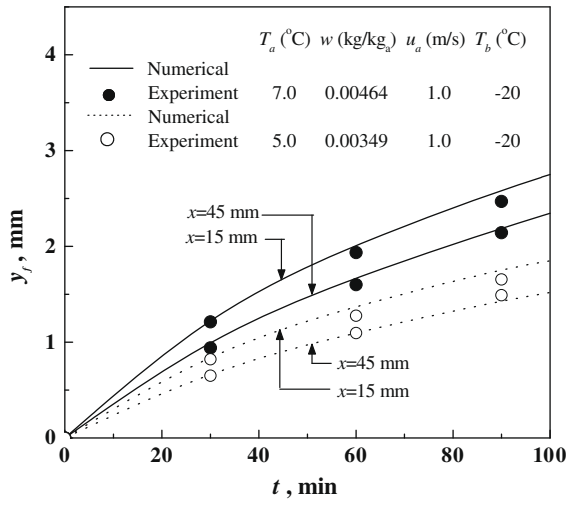

(a) The airflow direction at z = 35 mm

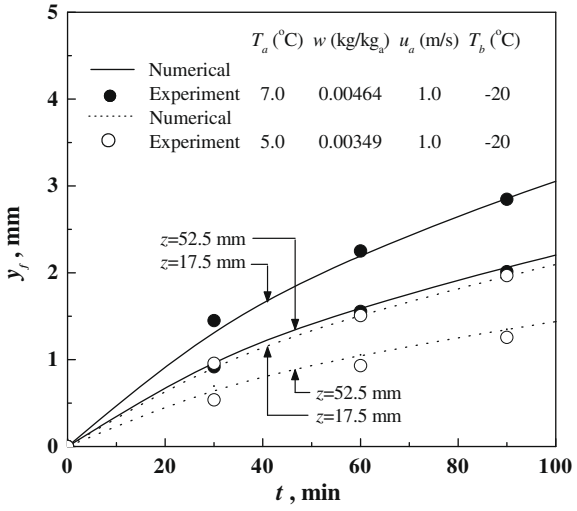

(b) The direction perpendicular to airflow at x = 30 mm

Fig. 6. Comparison of transient frost thickness between numerical results and experimental data, considering effects of humidity ratio.

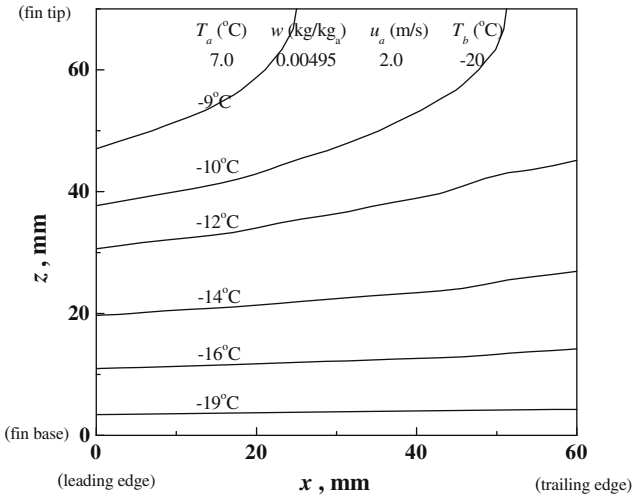

Fig. 7. Temperature contours on two-dimensional fin surface at t = 90 min.

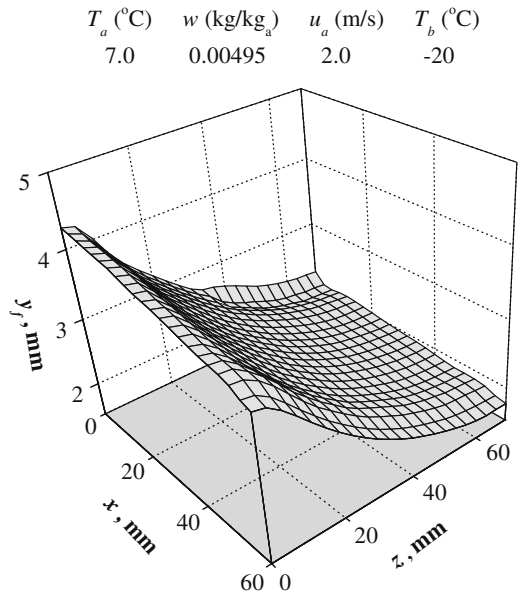

(a) frost thickness

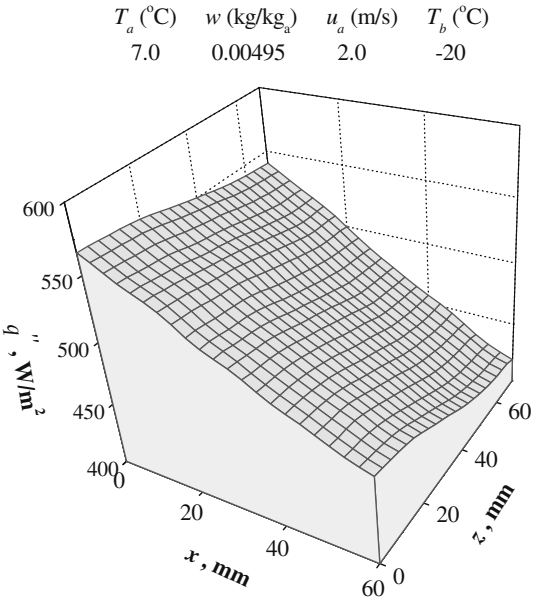

(b) heat flux

Fig. 8. Mapped surface for frost thickness and heat flux on a 2D fin at t = 90 min.

Fig. 8(a) shows the frost thickness distribution on a 2D fin at t = 90 min. In the z-direction, considerable frost growth was seen near the fin base due to fin heat conduction, and the frost thickness decreased exponentially toward the fin tip. Frost growth in the x-direction was active near the leading edge of the fin due to the leading edge effect, but decreased slightly toward the trailing edge of the fin. The variation of the frost growth in the x-direction was insignificant compared to that observed in the z-direction. Fig. 8(b) shows the heat flux on a 2D fin surface at t = 90 min. The heat transfer rate decreased toward the fin tip and also toward the trailing edge of the fin. In particular, the rate of decrease of heat transfer in the x-direction was high compared to that in the z-direction. This is because the temperature and humidity of the moist air diminished with its movement through the system, resulting in a decrease in the total heat transfer rate (sensible and latent heat) between the moist air and the interface.

4.2. The effects of fin heat conduction

Since the temperature gradient in the x-direction was small, we analyzed frost behavior in the z-direction at x = 30 mm by comparing two fin conditions: one with fin heat conduction (Case A) and the other with a constant fin surface temperature (Case B). The resulting frost thickness on the fin is shown in Fig. 9(a). The frost thickness decreased exponentially toward the fin tip in Case A, while it remained unchanged in Case B due to the almost constant properties of the moist air at x = 30 mm. At the maximum, the frost thickness in Case B was more than twice that of Case A. Fig. 9(b) shows the transient heat flux on the fin at a specific position, i.e. x = 30 mm and z = 35 mm. The heat flux in Case A was 10% lower on average than that of Case B due to the nonuniform temperature distribution and corresponding frost growth in Case A. Consequently, predictions of frost behavior made with the assumption of constant fin surface temperature might result in inaccurate results and degrade the reliability of the model. Therefore, consideration of the fin heat conduction would be essential to accurately predict frost behavior.

5. Equivalent temperature for the design of heat exchangers

Significant differences were seen in frost behavior with and without fin heat conduction. A concept of equivalent temperature was introduced to reconcile the difference between Case A and Case B. The equivalent temperature is defined as the temperature (constant in Case B) at which the heat transfer rate neglecting fin heat conduction is the same as the heat transfer rate with fin heat conduction taken into account. The concept of equivalent temperature could be applied to the design of heat exchangers, simplifying the analysis of frost behavior by avoiding the necessity of solving the complicated model with fin heat conduction taken into account. To predict frost behavior on heat exchanger fins at different operating conditions, we derived a correlation of equivalent temperature as a function of test conditions and geometrical dimensions. Based on Design of Experiment, numerical analyses were performed for 27 different conditions.

5.1. Equivalent temperature, T_{eq}

Fig. 10 shows the heat flux under the assumption of the constant fin temperature (T_c) (neglecting fin heat conduction) at t = 90 min. The heat transfer increased logarithmically as the constant fin temperature decreased. With fin heat conduction taken into account, the heat transfer rate at $T_b = -20$ °C was 493 W/m^2 (marked as point P), which was the same as the heat transfer rate at $T_c = -13$ °C neglecting fin heat conduction. The equivalent temperature was determined in this way, as illustrated by the broken arrow in Fig. 10.

5.2. Dimensionless correlation of equivalent temperature

To derive the correlation of equivalent temperature based on the heat transfer rate, we first calculated the equivalent temperatures for 27 different runs using the procedure described in the previous section. Through a dimensional analysis, a correlation of dimensionless equivalent temperature was expressed as a function of frosting parameters (air temperature, air velocity, air humidity ratio, fin base temperature, frosting time, constant fin surface temperature), geometrical dimensions (fin length, fin height, fin thickness) and air properties (density, viscosity, and thermal diffusivity).

$$F(T_a, u_a, w_a, T_b, t_{op}, T_c, L_{fin}, H_{fin}, t_{fin}, \rho_a, \mu_a, \alpha_a) = 0 \quad (11)$$

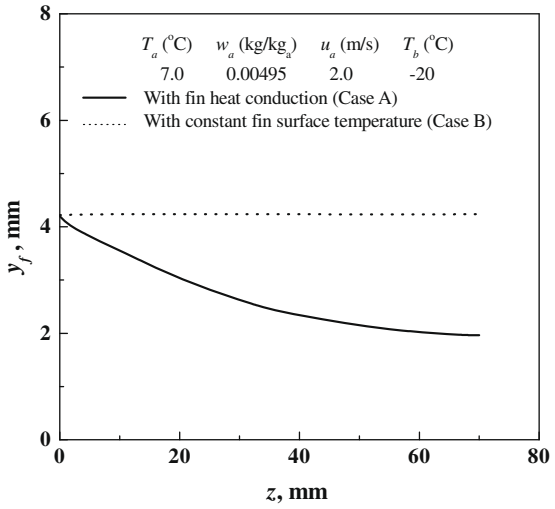

(a) Frost thickness at x=30 mm and t=90 min.

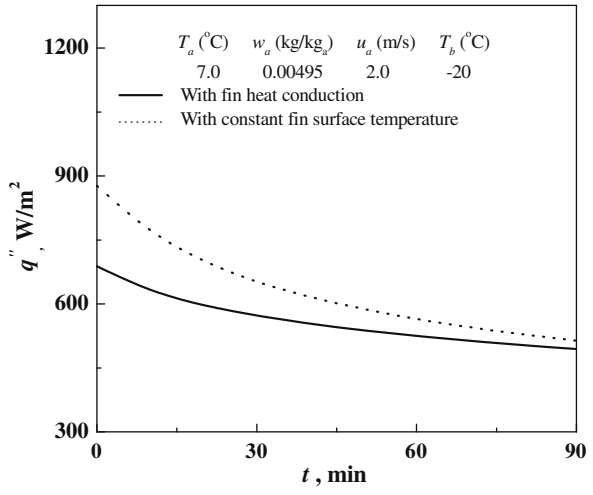

(b) Transient heat flux at x=30 mm and z=35 mm.

Fig. 9. Comparisons of frost thickness and transient heat flux with and without fin heat conduction.

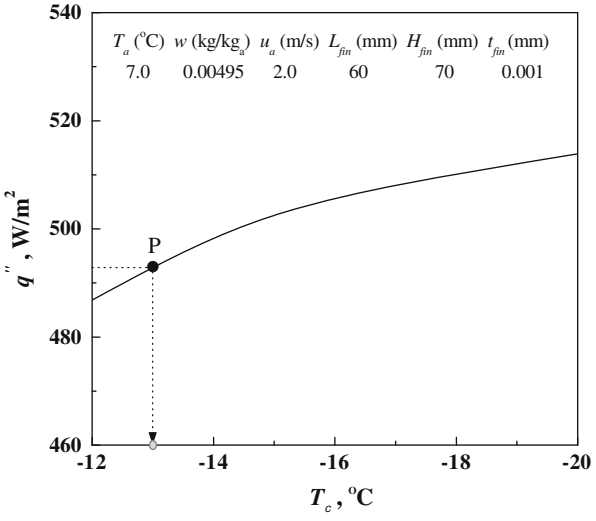

Fig. 10. Heat flux with variations of constant fin temperature for predicting equivalent temperature at t = 90 min.

By combining these variables, six nondimensional parameters were defined, i.e. dimensionless temperature, air humidity ratio, Reynolds number, Fourier number, ratio of fin height to fin length, and ratio of fin thickness to fin length.

$$T_c^* = \frac{T_c}{T_b} = G(T_a^*, w, \mathrm{Re_L}, \mathrm{Fo_L}, G_{fin}^*, t_{fin}^*) \tag{12a}$$

where

$$T_a^* = \frac{T_a}{T_b}, \quad \mathrm{Re_L} = \frac{u_a L_{fin}}{\nu}, \quad \mathrm{Fo_L} = \frac{\alpha_a t_{op}}{L_{fin}^2}, \quad G_{fin}^* = \frac{H_{fin}}{L_{fin}}, \quad t_{fin}^* = \frac{t_{fin}}{L_{fin}} \tag{12b}$$

The correlation of dimensionless equivalent temperature based on heat transfer rate was obtained by the least square method as follows:

$$T_c^* = \frac{T_{eq}}{T_b} = 0.83752 (T_a^*)^{0.14460} (w)^{0.00738} (\mathrm{Re_L})^{0.01584} (\mathrm{Fo_L})^{-0.00090} (G_{fin}^*)^{0.04457} (t_{fin}^*)^{-0.02015} \tag{13}$$

where T_{eq} represents the equivalent temperature of the fin. This correlation is valid when $277.15 \leqslant T_a \leqslant 283.15$ K, $0.00301 \leqslant w_a \leqslant 0.00608$ kg/kg$_a$, $1.0 \leqslant u_a \leqslant 2.0$ m/s, $0 \leqslant t_{op} \leqslant 90$ min, $243.15 \leqslant T_b \leqslant 253.15$ K, $40 \leqslant L_{fin} \leqslant 80$ mm, $50 \leqslant H_{fin} \leqslant 90$ mm, and $0.6 \leqslant t_{fin} \leqslant 1.4$ mm.

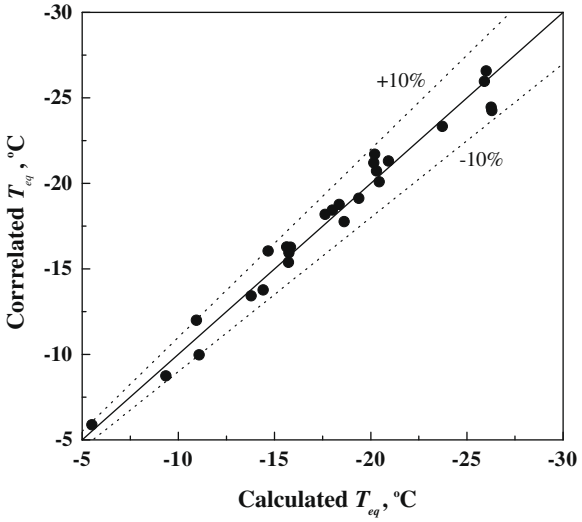

Fig. 11. Comparison of the calculated and correlated data of the equivalent temperature.

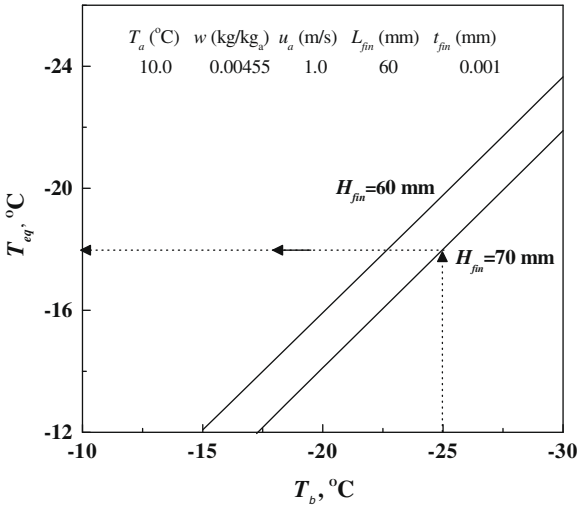

Fig. 12. Quantitative equivalent temperatures obtained from the correlation at t = 90 mm.

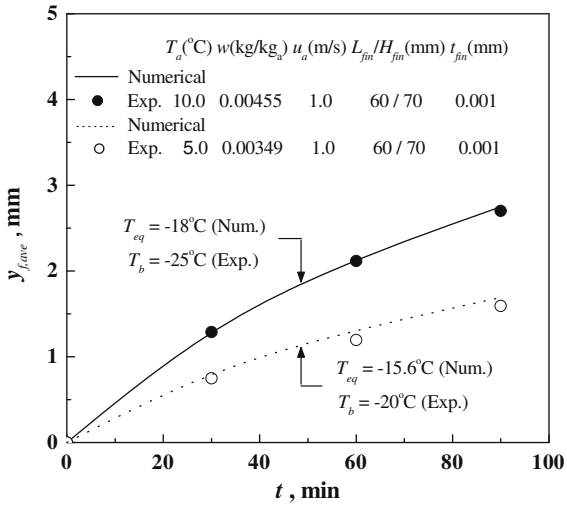

Fig. 13. Comparison of average frost thicknesses between the numerical for equivalent temperature and experiment, considering effects of humidity ratio.

Fig. 11 compares the calculated and correlated equivalent temperatures based on the heat transfer rate. The proposed correlation was in close agreement with the calculated data, with an error of less than 10%.

Fig. 12 shows the equivalent temperature, predicted by Eq. (13), as a function of the fin base temperature (T_b). The equivalent temperature decreased linearly as the fin base temperature decreased, regardless of fin height. When H_{fin} = 70 mm and T_b = −25 °C, the equivalent temperature was predicted to be −18 °C. Fig. 13 compares experimental average frost thicknesses with numerical results obtained by using the equivalent temperature, neglecting fin heat conduction, and considering effects of humidity ratio. The agreements were good. This indicates that the frost behavior of heat exchanger fins having a nonuniform temperature distribution could be effectively predicted by using the equivalent temperature and neglecting fin heat conduction.

6. Conclusions

A mathematical model was proposed to predict the frosting behavior and the characteristics of heat and mass transfer on a heat exchanger fin under frosting conditions, taking fin heat conduction into consideration. In this model, the change in the 3D airside airflow caused by frost growth was accounted for, since airside, frost layer, and fin model were coupled together. A frosting experiment was performed to validate the model. The numerical results agreed well with the experimental data, and the error was within 10%. Considerable frost growth occurred in the z-direction near the fin base due to fin heat conduction, and the frost thickness decreased exponentially toward the fin tip. Under the assumption of constant fin surface temperature, the frost thickness was larger by more than 200% at maximum and the heat flux by more than 10% on average, compared to results obtained with fin heat conduction taken into account. Thus, fin heat conduction must be considered to accurately predict frost behavior. The concept of equivalent temperature was introduced to make the simulation more valid under the assumption of constant fin surface temperature, and predictions that neglect fin heat conduction were shown to be reasonably accurate via use of the equivalent temperature. A correlation of equivalent temperature was derived that could be applied to the design of heat exchangers.

Acknowledgment

This work was supported by the research fund of Hanyang University (HY-2007-I).

References

[1] S.N. Kondepudi, D.L. O'Neal, Performance of finned-tube heat exchangers under frosting conditions. I. Simulation model, Int. J. Refrig. 16 (3) (1993) 175–180.
[2] D.K. Yang, K.S. Lee, S. Song, Modeling for predicting frosting behavior of a fin-tube heat exchanger, Int. J. Heat Mass Transfer 49 (7–8) (2006) 1472–1479.
[3] J. Martinez-Frias, S.M. Aceves, Modeling of a heat pump with evaporator air dehumidification for reduced frost formation, Trans. ASME (1998) 305–312.
[4] S. Jhee, K.S. Lee, W.S. Kim, Effect of surface treatments on the frosting/defrosting behavior of a fin-tube heat exchanger, Int. J. Refrig. 25 (8) (2002) 1047–1053.
[5] K. Kaygusuz, Performance of an air to air heat pump under frosting and defrosting conditions, Appl. Energy 48 (1994) 225–241.
[6] S.M. Sami, T. Duong, Mass and heat transfer during frost growth, ASHRAE Trans. 95 (1989) 158–165.
[7] K.A.R. Ismail, C.S. Salinas, Modeling of frost formation over parallel cold plates, Int. J. Refrig. 22 (5) (1999) 425–441.
[8] K.S. Lee, W.S. Kim, T.H. Lee, A one-dimensional model for frost formation on a cold flat surface, Int. J. Heat Mass Transfer 40 (18) (1997) 4359–4365.
[9] K.S. Lee, S. Jhee, D.K. Yang, Prediction of the frost formation on a cold flat surface, Int. J. Heat Mass Transfer 46 (2003) 3789–3796.
[10] H.C. Parish, C.F. Sepsy, A numerical analysis of frost formation under forced convection, ASHRAE Trans. (1972) 236–251.
[11] R. Yun, Y.C. Kim, M.K. Min, Modeling of frost growth and frost properties with airflow over a flat plate, Int. J. Refrig. 25 (2002) 362–371.
[12] Y.X. Tao, R.W. Besant, K.S. Rezkallah, A mathematical model for predicting the densification and growth of frost on a flat plate, Int. J. Heat Mass Transfer 36 (1993) 353–363.
[13] H. Chen, L. Thomas, R.W. Besant, Modeling frost characteristics on heat exchanger fins. Part I. Numerical model, ASHRAE Trans. (2000) 357–367.
[14] H. Chen, L. Thomas, R.W. Besant, Modeling frost characteristics on heat exchanger fins. Part II. Model validation and limitations, ASHRAE Trans. (2000) 368–376.
[15] C.P. Tso, Y.C. Cheng, A.C.K. Lai, An improved model for predicting performance of finned tube heat exchanger under frosting condition with frost thickness variation along fin, Appl. Therm. Eng. 26 (2006) 111–120.
[16] Y. Xia, A.M. Jacobi, An exact solution to steady heat conduction in a two-dimensional slab on a one-dimensional fin: application to frosted heat exchangers, Int. J. Heat Mass Transfer 47 (14–16) (2004) 3317–3326.
[17] M.N. Özisik, Heat Conduction, second ed., Wiley, New York, pp. 416–417.
[18] J.S. Kim, D.K. Yang, K.S. Lee, Dimensionless correlations of frost properties on a cold cylinder surface, Int. J. Heat Mass Transfer 51 (15–16) (2008) 3946–3952.
[19] S.J. Kline, F.A. McClintock, Describing uncertainties in single-sample experiments, Mech. Eng. 75 (1953) 3–8.